张秉峰，鲍学伟. 2023. 天山造山带壳幔结构与陆内变形机制研究进展. 地球与行星物理论评（中英文），54(1)：27-43. doi：10.19975/j.dqyxx.2022-048.
Zhang B F, Bao X W. 2023. Research progress on seismic structures of crust and mantle beneath Tien Shan and their geodynamic implications. Reviews of Geophysics and Planetary Physics, 54(1): 27-43 (in Chinese). doi:10.19975/j.dqyxx.2022-048.

天山造山带壳幔结构与陆内变形机制研究进展

张秉峰，鲍学伟*
浙江大学地球科学学院 浙江省地学大数据与地球深部资源重点实验室，杭州 310027

摘要：天山作为当今世界上最为典型的陆内造山带，对于其深部结构和新生代构造变形过程的研究一直是地球科学领域的前沿和热点，并已经取得大量成果. 本文系统总结了近年来利用地震学方法对天山造山带及其邻区壳幔结构研究的最新进展以及存在的争议. 这些研究发现包括地壳厚度、莫霍面形态、地幔转换带厚度、地震波速、Q 值结构在内的多结构参数的变化与区内各个大地构造单元的对应性较好，彰显出盆-山深部结构的显著差异. 研究区各向异性结构复杂，地壳内部的偏振方向存在明显的横向变化，并在上地幔深度转换为和造山带走向基本一致. 另外，在中下地壳和上地幔顶部，天山大部表现为明显的低速异常. 以上结果揭示了陆内俯冲和地幔上涌对于塑造现今天山复杂构造格局与地质地貌特征的重要意义. 然而，现有研究对于我国新疆境内天山壳幔各向异性、岩石圈底界面以及地幔转换带的分辨率还远远不够，并且对于一些重要的结构参数及其解释尚未达成一致的认识. 密集流动地震台阵观测和多种地球物理资料的联合分析是解决这一问题并增进对陆内造山带深部动力学过程认识的有效途径.

关键词：天山；壳幔结构；各向异性；陆内造山
doi：10.19975/j.dqyxx.2022-048 **中图分类号**：P315 **文献标识码**：A

Research progress on seismic structures of crust and mantle beneath Tien Shan and their geodynamic implications

Zhang Bingfeng, Bao Xuewei*

Key Laboratory of Geoscience Big Data and Deep Resource of Zhejiang Province,
School of Earth Sciences, Zhejiang University, Hangzhou 310027, China

Abstract: The mechanisms causing the uplifting of the Tien Shan, one of the largest and most active intracontinental orogenic belts on Earth, have been vigorously debated for decades. Seismic investigation is a fundamental tool used for deep structural exploration and is key to understanding continental geodynamics. As such, in this study, we reviewed the recent research progress on the crustal and upper-mantle structures of the Tien Shan and the remaining controversies. The results showed that the Tien Shan and adjacent basins exhibit contrasting structural and physical properties from the crust down to the upper mantle in various aspects, such as crustal thickness, Moho morphology, mantle transition-zone thickness, seismic velocity, and seismic attenuation. The mountainous areas have complex crustal seismic anisotropy patterns, whereas orogen-parallel anisotropic fabrics dominate at upper mantle depths. Low-velocity anomalies pervasively exist in the mid-lower crust and uppermost mantle of Tien Shan. Taken together, these observations provide evidence of the important roles played by intracontinental subduction and mantle upwelling in Cenozoic orogenesis of the Tien Shan. However, further development of our under-

收稿日期：2022−05−20；**录用日期**：2022−06−28
基金项目：国家重点研发计划资助项目（2019YFA0708604）；国家自然科学基金资助项目（41774045）
Supported by the National Key Technologies R&D Program (Grant No. 2019YFA0708604) and the National Natural Science Foundation of China (Grant No. 41774045)
第一作者：张秉峰（1996-），男，博士研究生，主要从事天然地震学研究. E-mail：bingfeng.zhang@zju.edu.cn
***通信作者**：鲍学伟（1985-），男，研究员，主要从事地震学研究. E-mail：xwbao@zju.edu.cn

standing of the geodynamics in Tien Shan has been hindered by the low imaging resolution of seismic anisotropy, lithosphere-asthenosphere boundary, and mantle transition zone in eastern Tien Shan. And some important geophysical parameters and their implications are still far from being well-understood. Future deployment of dense temporary seismic arrays in the eastern Tien Shan and joint inversion of multiple and complementary geophysical data will considerably increase the resolution of seismic models and ultimately enhance our knowledge of geodynamic evolution in compressional intracontinental orogens.

Keywords: Tien Shan; crustal and upper-mantle structure; seismic anisotropy; intracontinental orogenesis

0　引　言

印度-亚洲碰撞造山作为新生代全球最重要的地质事件（Molnar and Tapponnier, 1975），不仅造成了喜马拉雅-青藏高原的抬升，也形成了世界上最年轻和最活跃的陆内造山带——天山（Sobel and Dumitru, 1997; Yin et al., 1998）. 天山造山带主体位于塔吉克斯坦、吉尔吉斯斯坦和我国新疆地区，其东西向跨度约 2 500 km，由一系列平行排列的山脉和山间盆地构成，海拔最高处的托木尔峰达 7 443 m. 作为中亚造山带和环青藏高原盆山体系（贾承造等, 2008; Xiao et al., 2020）的重要组成部分，天山夹持于南侧的塔里木盆地、帕米尔高原与北侧的准噶尔盆地、哈萨克地盾之间，通常以塔拉斯—费尔干纳断裂和 80°E 为界，划分为西、中、东三个段落（Lei, 2011）（图 1）.

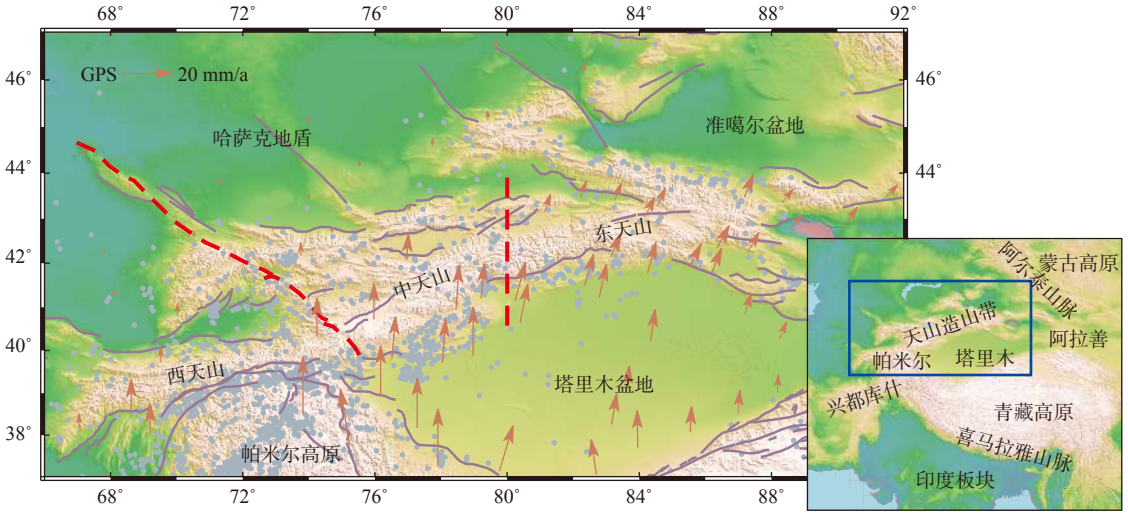

图 1　天山造山带及其邻区的地质构造背景. 灰色实线为研究区主要断层（数据来自 Styron and Pagani, 2020），红色虚线为塔拉斯—费尔干纳断裂和 80°E 经线，灰色圆圈表示 1964 年以来发生的 5 级以上强震分布，橙色箭头表示以欧亚大陆为参考系的地表运动速度场（数据来自 Gan et al., 2007; Zubovich et al., 2010）

Fig. 1　Tectonic map of Tien Shan and surrounding areas. Gray solid lines show major fault traces from Styron and Pagani (2020). Red dashed lines mark locations of Talas-Fergana fault and 80° E, which are boundaries between different segments of Tien Shan. Gray circles show distribution of large earthquakes (M_b>5) that have occurred since 1964. Orange arrows denote GPS velocities relative to Eurasia (data from Gan et al., 2007; Zubovich et al., 2010)

天山作为复活型陆内造山带，主要经历两期次的强构造活动. 古天山形成于海西期岛弧、微陆块等构造单元的多期次碰撞增生造山过程，其变形一直持续到中生代（Burtman, 1975）. 新生代以来，在印度—欧亚板块碰撞的远程效应下，已被夷平的早期造山带再次经历强烈隆升和构造变形作用（Sobel and Dumitru, 1997; Yin et al., 1998）. 现今天山正以 10～20 mm/a 的速率缩短，地壳缩短总量达 50～203 km，且不同段落的汇聚变形呈现出明显的差异性（Avouac et al., 1993; Makarov, 1995; Zhang et al., 2004; Gan et al., 2007; Zubovich et al., 2010; Li J et al., 2016; Zhang et al., 2020）. 研究区地震活动性强，尤其是新疆伽师和帕米尔地区中强震频发并具有较高的潜在地震危险性（高国英等, 2010; Sippl et al., 2013），更加显现了研究天山深部结构的重要意义. 帕米尔的北向挤入（Kufner et al., 2016）、塔里木的顺时针旋转（Avouac et al., 1993）、天山山脉宽度和缩短速率的东西向差异（Reigber et al., 2001）一方面彰显了新生代天山构造环境和地球动力学过程的复杂性，另一方面也使

得天山成为研究陆内造山过程的理想场所.

为探索天山新生代隆升的动力学机制，近年来国内外学者在天山造山带及其周缘实施了一系列深部结构探测和研究计划（熊小松等，2011；雷显权等，2012），利用人工地震测深和宽频地震探测方法，获得了从地表到地幔过渡带的多层次、多尺度的结构信息. 本文综合总结这些地震探测结果，梳理了当前科学界对于研究区深部结构的共识以及仍有争议的一些问题，并以此为基础对天山新生代陆内造山的深部变形响应进行了探讨.

1　壳幔主要速度间断面几何形态特征

1.1　莫霍面

莫霍面作为地壳和上地幔的分界面，通常受到深部构造活动的改造作用，其形态和结构特征是解析天山隆升过程的关键信息. 综合远震接收函数、人工地震剖面、重力资料反演等研究成果，我们发现天山造山带及其邻区的地壳厚度和地表高程存在明显的相关性（图 2a）. 高海拔的天山山脉和帕米

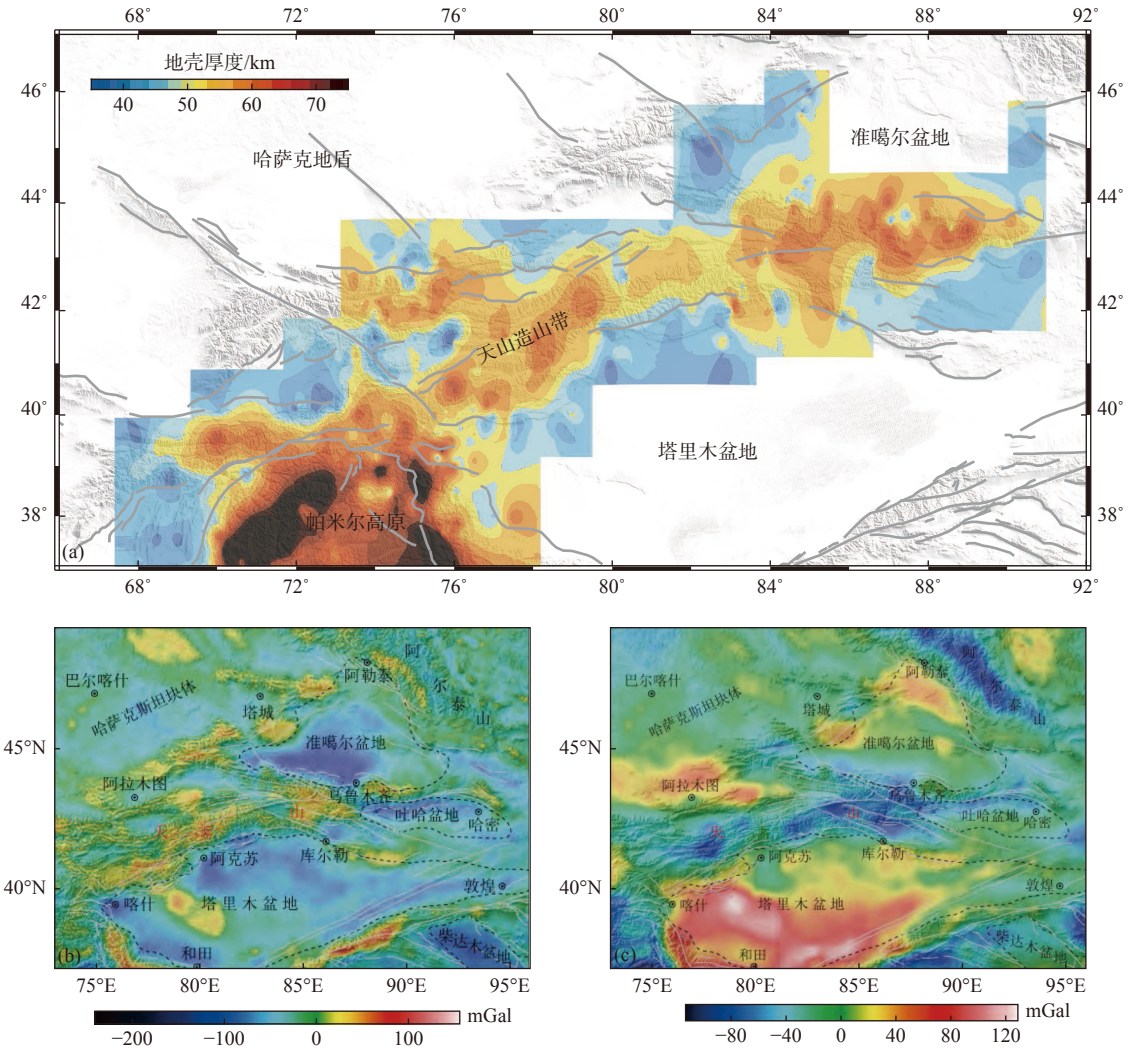

图 2　天山及邻区的地壳厚度和均衡重力异常.（a）接收函数方法约束的地壳厚度结果（整合自 Bump and Sheehan, 1998; Vinnik et al., 2006; 李昱等, 2007; Chen et al., 2010; 刘文学等, 2011; Schneider et al., 2013; He C et al., 2014; He R et al., 2014; 唐明帅等, 2014; Li Y et al., 2016; 郑雪刚等, 2016; Wu et al., 2018; Schneider et al., 2019; Zhang et al., 2020; Cai et al., 2021; Xu et al., 2021; Cheng et al., 2022; Cui et al., 2022），经克里金插值得到.（b）Airy 均衡重力异常（修改自张星宇等，2020）.（c）Vening-Meinesz 均衡重力异常（修改自张星宇等，2020）

Fig. 2　Crustal thickness and isostatic gravity anomaly of Tien Shan and its surroundings. (a) Crustal thickness measurements from receiver-function studies interpolated using Kriging method (compiled from Bump and Sheehan, 1998; Vinnik et al., 2006; Li et al., 2007; Chen et al., 2010; Liu et al., 2011; Schneider et al., 2013; He C et al., 2014; He R et al., 2014; Tang et al., 2014; Li Y et al., 2016; Zheng et al., 2016; Wu et al., 2018; Schneider et al., 2019; Zhang et al., 2020; Cai et al., 2021; Xu et al., 2021; Cheng et al., 2022; Cui et al., 2022). (b) Airy isostatic gravity anomaly (modified from Zhang et al., 2020). (c) Vening-Meinesz isostatic gravity anomaly (modified from Zhang et al., 2020)

尔高原的地壳较厚，分别为 50～65 km 和 65～75 km；低海拔的哈萨克南缘、准噶尔南缘、塔里木北缘以及山间盆地（如费尔干纳、纳伦、伊塞克湖、焉耆、库米什、吐哈）的莫霍面则相对较浅，一般位于 40～50 km 深度（Bump and Sheehan, 1998; Oreshin et al., 2002; Zhao et al., 2003; Vinnik et al., 2004; Kumar et al., 2005; 李顺成等, 2005; 米宁等, 2005; Vinnik et al., 2006; 李昱等, 2007; Shin et al., 2007; Chen et al., 2010; 刘文学等, 2011; Steffen et al., 2011; 侯贺晟等, 2012; Gao et al., 2013; Gilligan et al., 2014; He C et al., 2014; He R et al., 2014; 刘文学等, 2014; 唐明帅等, 2014; Li J et al., 2016; Li Y et al., 2016; 郑雪刚等, 2016; Guy et al., 2017; Wu et al., 2018; 蔡妍等, 2019; Schneider et al., 2019; Lü et al., 2020; Zhang et al., 2020; Cai et al., 2021; Xu et al., 2021; Cheng et al., 2022; Cui et al., 2022）.

观测莫霍面与理论均衡补偿面的深度差异反映区域地壳均衡状态，天山及邻区的相关研究结果差异显著，主要原因在于设定的均衡补偿模式不同. 基于 Airy 局部均衡理论的计算结果一般认为天山地壳呈现均衡正异常（莫霍面深度小于均衡补偿深度），两侧盆地以均衡负异常为主（Balmino et al., 2012; Li Y et al., 2016; Cai et al., 2021）（图 2b）. 相比之下，根据 Vening-Meinesz 区域均衡理论或者考虑到地壳内部结构特征获得的均衡状态被认为在物理上更符合实际情况，山区大部表现为均衡负异常，盆地则以均衡正异常为特征（Steffen et al., 2011; Kaban and Yuanda, 2014; Guy et al., 2017; 张星宇等, 2020）（图 2c），均衡调整方向和区域地壳垂向运动趋势一致（赵静旸等，2019）.

天山和两侧盆地莫霍面的另一显著差异在于其结构和形态特征. 准噶尔南缘和塔里木北缘的壳幔界面表现为一级速度间断，形态上接近水平；而天山山脉尤其是其南北山麓地带则以缓变的速度梯度带或多薄层结构为主，并广泛存在错断（Moho offset）和双莫霍面（Moho Doublet）等复杂构造（Zhao et al., 2003; 李顺成等, 2005; 米宁等, 2005;李昱等, 2007; 侯贺晟等, 2012; Gao et al., 2013; He C et al., 2014; Li J et al., 2016; Li Y et al., 2016; 蔡妍等, 2019; Zhang et al., 2020）. 另外，接收函数偏移成像研究表明天山内部的莫霍面形态可能具有系统性差异（Li J et al., 2016; Zhang et al., 2020）（图 3）. 北天山以南倾的双莫霍面为主要特征，对应哈萨克和准噶尔的南向俯冲；南天山的莫霍面在山脉中段向南倾斜并在盆山结合部发生错断，在东段则位于相对较浅的深度并存在多个错断，表明南天山地壳在塔里木向北推挤作用下发生缩短增厚变形并且变形强度存在东西向差异，可能和天山东段的汇聚速率较小有关（Reigber et al., 2001）.

1.2　岩石圈-软流圈边界

S 波接收函数由于其不受浅层多次波干扰的特性，常用于岩石圈-软流圈边界（lithosphere-asthenosphere boundary, LAB）起伏形态的探测. 相关研究结果表明天山中段的岩石圈厚度约为 90～120 km，相对于北侧哈萨克（约 130 km）和南侧塔里木（约 160～180 km）发生明显减薄，推测存在从喀喇昆仑到天山的软流圈物质上涌通

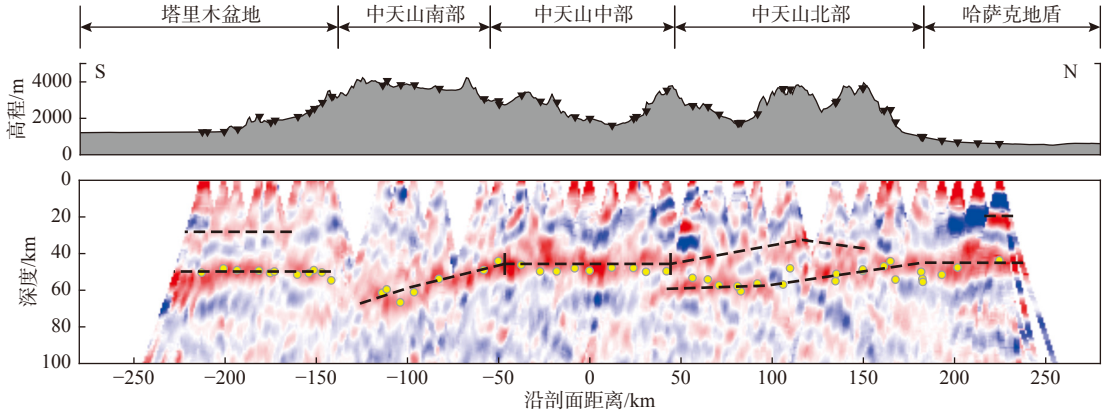

图 3　天山造山带中段的莫霍面形态（修改自 Zhang et al., 2020）. 黑色倒三角为地震台站，黄色圆圈表示由接收函数叠加网格搜索（*H*-*κ*-*c*）获得的各台站下方莫霍面深度，黑色虚线表示由接收函数共转换点叠加（CCP）揭示的莫霍面几何形态

Fig. 3　Moho morphology of central Tien Shan (modified from Zhang et al., 2020). Seismic stations are marked as black inverted triangles. Yellow circles denote Moho depth measurements from a stacking and grid search scheme on receiver functions (*H*-*κ*-*c*); black dashed lines show preferred Moho geometry from CCP image

道（Oreshin et al., 2002; Kumar et al., 2005）（图 4a）. 另外，Pasyanos 等（2014）通过对面波频散数据的拟合认为天山岩石圈可能具有强烈的横向不均一性，天山东部岩石圈显著增厚（约 190 km）. Zhao 等（2003）根据巴音布鲁克—布尔津剖面的壳幔电性结构也获得了类似的岩石圈厚度估计（约 160～180 km），但由于面波和大地电磁对于速度间断面的分辨率较低，该推测仍需进一步确认.

1.3　地幔转换带上下界面

地幔转换带（mantle transition zone, MTZ）是上下地幔物质运移和能量交换的场所，其上下界面（410-km 和 660-km 间断面）的起伏与温度场以及物质成分的变化密切相关（Helffrich, 2000; Wu et al., 2022）. 因而准确约束地幔转换带的厚度及其界面形态对于认识天山构造活动的作用深度和动力来源具有重要意义. 现有的研究结果主要集中在天山中段（Chen et al., 1997; Tian et al., 2010; He C et al., 2014; Lessing et al., 2014; 高雅健等, 2017; Yu et al., 2017; Kosarev et al., 2018; Vinnik et al., 2018）（图 4b）. 一般认为山体下方的地幔转换带增厚约 3～20 km，与该深度的高速异常体有较好的对应关系（Lei and Zhao, 2007; Li et al., 2009），反映在碰撞造山过程中拆沉的岩石圈已经到达地幔转换带深度. 另外，哈萨克南缘、塔里木北缘以及费尔干纳盆地下方的地幔转换带存在约 7～20 km 的减薄，可能与局部热物质上涌或地幔柱相关. 值得一提的是，虽然不同研究获得的转换带厚度变化特征大体相近，但由于研究方法、数据来源、以及参考模型的不同，对于 410-km 和 660-km 间断面起伏形态的认识仍存在较大差异. 另一个争议点在于天山下方的拆沉体的属性，是对流减薄的天山岩石圈地幔还是俯冲并剥离的塔里木或哈萨克岩石圈仍不十分清楚（Tian et al., 2010; Yu et al., 2017）.

2　地震各向异性与壳幔形变特征

利用地震波在各向异性介质中的传播特性来解析地球介质的各向异性结构是探测深部变形过程的重要手段，并且一般认为裂隙、矿物和熔体的定向排列以及薄互层结构是地震各向异性的直接来源（Crampin, 1994; Zhang and Karato, 1995; 杨彧等, 2010; Ko and Jung, 2015）. 其中剪切波分裂（Silver and Chan, 1991）作为最常用的研究方法，当台站密度较大时可获得较高的横向分辨率，虽然垂向分辨率有限，但可以通过引入多种类型剪切波进行改善（如 SKS/SKKS、Pms、S）. 另外，针对 P/Pn 波走时（Hearn, 1996; Liang et al., 2004; Wang and Zhao, 2008）、接收函数/SKS 波形（Vinnik et al., 2002），以及面波频散等数据的反演研究（Bao et al., 2016, 2020; Malory et al., 2022）解析的各向异性结构往往具有较高的垂向分辨率，其中后者还可以通过比较瑞利波和勒夫波的速度结构获得径向各向

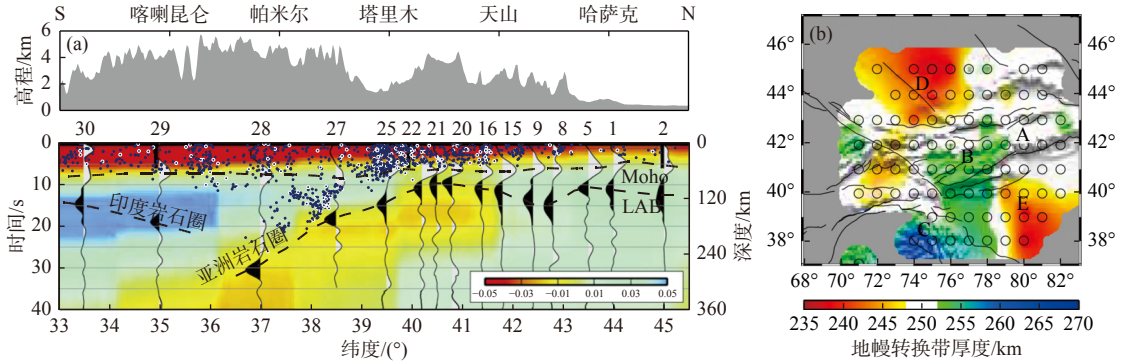

图 4　天山造山带中段的岩石圈-软流圈间断面形态和地幔转换带厚度.（a）S 波接收函数约束的岩石圈-软流圈间断面形态（修改自 Kumar et al., 2005）. 蓝色圆圈表示测线附近的地震分布，背景 S 波速度异常由地震面波层析成像获得（Friederich, 2003）.（b）P 波接收函数约束的地幔转换带厚度变化（修改自 Yu et al., 2017）. 黑线表示断层分布，圆圈为反投影处理中使用的 1°×1°网格

Fig. 4　LAB morphology and MTZ thickness beneath central Tien Shan. (a) LAB morphology constrained by S-wave receiver-function imaging (modified from Kumar et al., 2005). Blue circles are earthquake hypocenters within a 100 km wide zone along the seismic profile. Background S-wave velocities are based on surface-wave tomography images reported by Friederich (2003). (b) Smoothed spatial distribution of MTZ thickness constrained by P-wave receiver-function imaging (modified from Yu et al., 2017). Black lines are major active faults. Open circles show locations of bins used during backprojection of receiver functions

异性信息. 因此对天山山脉采用不同方法约束的地震各向异性结构进行梳理有助于加深我们对于陆内造山动力学过程的认识.

SKS/SKKS 分裂反映了台站下方从地表到核幔边界的平均各向异性结构，相关研究结果对天山中西段覆盖较好，在天山东段主要集中在乌鲁木齐—库尔勒公路沿线（图 5a）. 整体上看，快波偏振方向（NEE-SWW）和造山带走向近似平行，约 1 s 的分裂时间表明山体下方变形作用较强（Silver and Chan, 1991; Makeyeva et al., 1992; Vinnik et al., 1992; Helffrich et al., 1994; Wolfe and Vernon III, 1998; Barruol and Hoffmann, 1999; Iidaka and Niu, 2001; Chen et al., 2005; Li and Chen, 2006; 江丽君等, 2010; Li et al., 2010; Huang et al., 2011; 冯强强等, 2012; Cherie et al., 2016; 孙吉泽等, 2016; Kufner et al., 2018）. 然而，迄今为止对于该特征所指示的地球动力学过程尚未达成统一的认识，南北向挤压引起的岩石圈缩短增厚、大规模地幔对流或软流圈物质的侧向流动、板块运动相关的矿物定向排列等模式相继被提出，古生代汇聚造山过程中残余的化石各向异性（fossil anisotropy）也被认为对观测结果有一定贡献. 在这个 SKS/SKKS 各向异性和山脉走向平行的大背景下，多项研究在伊塞克湖及其周缘发现有异常的快波偏振方向（NNE-SSW），可能与局部的地幔对流/地幔柱活动有关（Makeyeva et al., 1992; Wolfe and Vernon III, 1998; 江丽君等, 2010）；但也有研究指出该观测结果受限于数据较差的方位角覆盖（局限在 90°～110°方位），不足以反映伊塞克湖地区的平均各向异性结构（Cherie et al., 2016）. 值得一提的是，类似的异常各向异性特征在塔拉斯—费尔干纳断裂附近和中天山南部山麓地带也有发现（Li and Chen, 2006; Kufner et al., 2018），但考虑到数据量较少，需谨慎考虑其可能的成因.

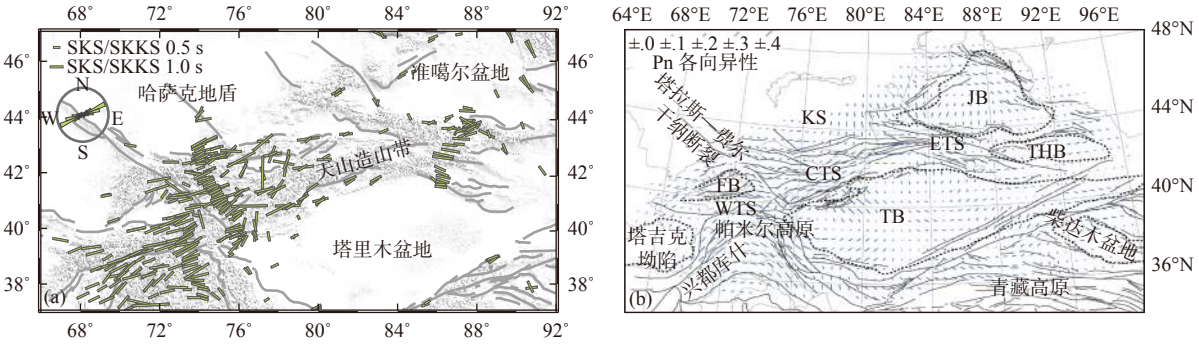

图 5　天山及邻区的地幔各向异性. （a）SKS/SKKS 分裂获得的壳幔综合各向异性分布（整合自 Silver and Chan, 1991; Makeyeva et al., 1992; Vinnik et al., 1992; Helffrich et al., 1994; Wolfe and Vernon III, 1998; Barruol and Hoffmann, 1999; Iidaka and Niu, 2001; Chen et al., 2005; Li and Chen, 2006; 江丽君等, 2010; Huang et al., 2011; 冯强强等, 2012; Cherie et al., 2016; Kufner et al., 2018; Gao and Sun, 2021; Zhang et al., 2022）. 绿色短棒的方向和长度分别表示快剪切波偏振方向和快慢波分裂时间. （b）Pn 波层析成像获得的上地幔顶部各向异性分布（修改自 Zhou and Lei, 2015）. 蓝色短棒的方向和长度分别表示快剪切波传播方向和各向异性强度，虚线为研究区主要沉积盆地轮廓，实线为研究区主要断层. TB：塔里木盆地，JB：准噶尔盆地，KS：哈萨克地盾，FB：费尔干纳盆地，WTS：西天山，CTS：中天山，ETS：东天山，THB：吐哈盆地

Fig. 5　Upper-mantle seismic anisotropy of Tien Shan and its surroundings. (a) SKS/SKKS anisotropy targeting both crust and upper mantle (compiled from Silver and Chan, 1991; Makeyeva et al., 1992; Vinnik et al., 1992; Helffrich et al., 1994; Wolfe and Vernon III, 1998; Barruol and Hoffmann, 1999; Iidaka and Niu, 2001; Chen et al., 2005; Li and Chen, 2006; Jiang et al., 2010; Huang et al., 2011; Feng et al., 2012; Cherie et al., 2016; Kufner et al., 2018; Gao and Sun, 2021; Zhang et al., 2022). Fast polarization axis and amount of splitting are indicated by orientation and length of bar line, respectively. (b) Pn anisotropy targeting uppermost mantle (modified from Zhou and Lei, 2015). Fast-propagation direction and strength of anisotropy are indicated by orientation and length of bar line, respectively. Black dashed lines are outlines of major sedimentary basins; black solid lines indicate major active faults. TB, Tarim basin; JB, Junggar basin; KS, Kazakh shield; FB, Fergana basin; WTS, western Tien Shan; CTS, central Tien Shan; ETS, eastern Tien Shan; THB, Turpan-Hami basin

SKS/SKKS 分裂结果随方位角的周期性变化特征和针对接收函数/SKS 波形的反演方法常用于刻画台站下方的双层（复杂）各向异性结构. 结果显示，天山中段的部分台站以及位于天山东段的 WMQ 台站下方可能存在双层各向异性结构（Farra et al., 1991; Vinnik et al., 2002; Vinnik et al., 2007; Li et al., 2010; Huang et al., 2011; Cherie et al., 2016），但不同研究获得的结构参数差异明显. 以 WUS 台站为例，Cherie 等（2016）和 Li 等（2010）的研究结果显示该台站上层和下层的各向异性方向分别

为 NEE-SWW 和 NWW-SEE；另一方面，Vinnik 等（2002）、Vinnik 等（2007）及 Farra 等（1991）则获得了完全相反的结果，认为上层和下层各向异性分别位于 NWW-SEE 和 NEE-SWW 方向. 值得注意的是，由于天山地区地震台站记录的 SKS/SKKS 数据方位分布不均，通过拟合 SKS/SKKS 分裂结果随方位角的变化规律获得的双层各向异性参数往往稳定性较差并具有多解性. 此外，下地幔低剪切速度区边缘地带的强烈各向异性也可能对 SKS/SKKS 各向异性的扰动有贡献，比如 Zhang 等（2022）发现天山中段偏离造山带走向的各向异性观测结果，在 2 700 km 深度的穿透点大多位于 Perm Anomaly 边界，暗示可能存在一定关联性.

Pn 波走时反演能够约束上地幔顶部的各向异性结构. 天山及其邻区的相关研究结果显示（图 5b），上地幔顶部的各向异性方向在山脉主体表现为和造山带走向平行，一般认为受到岩石圈缩短变形过程的控制，另外地幔热物质的上涌也被认为对该特征有一定贡献；而在天山中东段的盆山结合部则以垂直造山带走向为特征，推测可能和两侧块体向天山方向的俯冲有关（李志伟等, 2007; Zhou and Lei, 2015; He et al., 2019）.

在 SKS/SKKS 分裂研究中，一般认为地壳变形的贡献较小，各向异性层主要分布在岩石圈地幔和软流圈内部. 但这一假设对于经历强烈地壳缩短和快速隆升的天山造山带可能并不成立（Vinnik et al., 2002, 2007; Chen et al., 2005）. Pms 分裂结果反映了台站下方地壳平均的各向异性结构，一项针对天山中段 MANAS 测线的 SKS/SKKS 和 Pms 分裂研究结果显示（图 6a），天山地壳各向异性较强（约 0.6 s），相比于 SKS/SKKS 震相约 1.0 s 的分裂时间，表明天山地区地壳/岩石圈变形对于 SKS/SKKS 分裂具有重要贡献（Zhang et al., 2022）. 该项研究同时揭示了天山各向异性结构的横向差异，南天山以平行山脉走向的快波偏振方向为特征，对应塔里木北向推挤造成的整个南天山岩石圈的纯剪切变形；而北天山的地壳各向异性主要表现为与塔里木—哈萨克汇聚方向平行，可能与哈萨克下地壳南向俯冲引起的简单剪切变形有关（Zhang et al., 2022）.

对近震 S 波进行剪切波分裂分析可以进一步将各向异性深度限制在上地壳. 对于天山地区，近震 S 波的快波偏振方向一般与主压应力方向或相邻断裂走向平行，反映上地壳各向异性和区域构造以及应力场密切的关联性；快慢波分裂时间较小

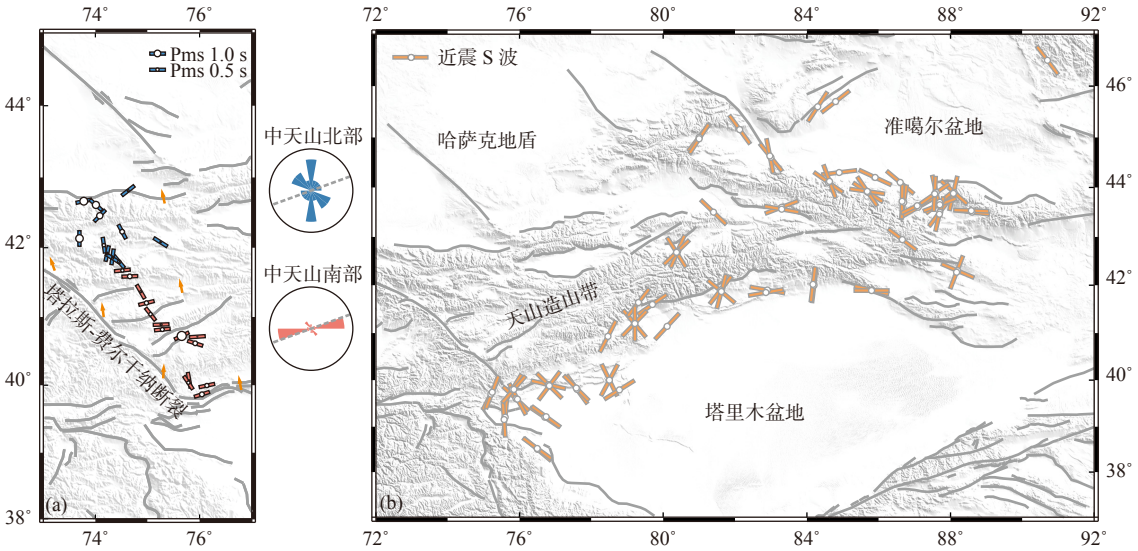

图 6　天山及邻区的地壳各向异性.（a）接收函数 Pms 分裂获得的地壳各向异性分布（修改自 Zhang et al., 2022）. 短棒的方向和圆圈的大小分别表示快剪切波偏振方向和快慢波分裂时间，橙色箭头表示原地最大水平压应力方向（Heidbach et al., 2018），玫瑰图中虚线表示天山山脉走向.（b）近震 S 波分裂获得的上地壳各向异性分布（整合自鲍子文和高原, 2017; Li et al., 2021）. 短棒的方向表示快剪切波偏振方向

Fig. 6　Crustal seismic anisotropy of Tien Shan and its surroundings. (a) Pms anisotropy targeting the crust (modified from Zhang et al., 2022). Fast-polarization axis and amount of splitting are indicated by bar line orientation and circle size, respectively. Orange arrows indicate maximum horizontal compressional stress direction (Heidbach et al., 2018). Dashed lines in rose diagrams denote strike of Tien Shan. (b) Local S-wave anisotropy targeting upper crust (compiled from Bao and Gao, 2017; Li et al., 2021). Fast-polarization axis is demonstrated by bar line orientation

（<0.2 s），表明地壳各向异性主要来源于中下地壳矿物晶格的优势排列（Wolfe and Vernon III, 1998; 赖院根等, 2002; 高歌和王海涛, 2006; 鲍子文和高原, 2017, 2019）（图 6b）. 在中下地壳深度，基于背景噪声频散的反演研究发现，快波偏振方向在伊塞克湖附近偏转为近似垂直于山脉走向，和该区域 SKS/SKKS 分裂结果一致，推断地幔热物质可能上涌到地壳深度（Guo et al., 2017）. 此外，关于天山造山带径向各向异性的研究目前仍较为初步，成像结果差异较大（周铭等, 2014; Liang et al., 2020）.

3　壳幔三维地震波速度结构

应用地震层析成像方法可揭示天山造山带及其邻区包括 P 波、S 波、瑞利波和勒夫波在内多种类型地震波的三维速度结构，研究结果表明天山地壳上地幔具有明显非均匀性. 在上地壳深度、速度结构与地表构造有很好的对应关系（图 7a）. 在沉积层相对较厚的塔里木、准噶尔、哈萨克地区以及部分山间盆地（如费尔干纳、纳伦、伊塞克湖）表现为显著的低速异常，其中准噶尔盆地低速层的厚度向南逐渐增大，可能与北天山隆升以及准噶尔沉降过程相关；而山脉主体部分由于受到古生代结晶基底抬升的影响，一般具有较高的地震波速度（Xu et al., 2002; Zhao et al., 2003; Omuralieva et al., 2009; Guo et al., 2010; Zheng et al., 2010; Lei, 2011; Gao et al., 2014; Gilligan et al., 2014; Bao et al., 2015; Li Y et al., 2016; Guo et al., 2017; Li et al., 2018; Lü et al., 2019; Aminov et al., 2020; 孔祥艳等, 2021）.

在中下地壳深度（图 7b），天山中东段整体波速较低，低速异常广泛分布，虽然部分研究在纳伦和伊塞克湖地区发现有与古生代碰撞过程相关的高速体（Kosarev et al., 1993; Xu et al., 2002; Zhao et

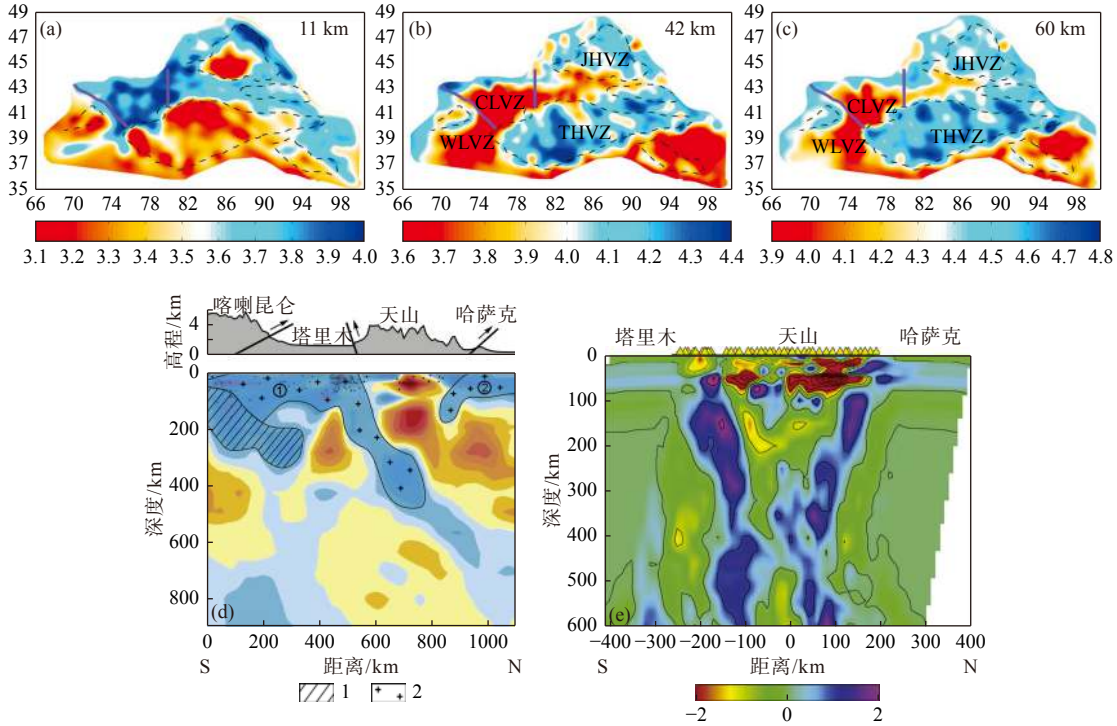

图 7　天山及邻区的壳幔地震波速度结构. （a-c）背景噪声全波形反演获得的 11-km、42-km 和 60-km 深度 S 波速度水平切片（修改自 Lü et al., 2019）. 紫色实线为塔拉斯—费尔干纳断裂和 80°E 经线，黑色虚线为研究区主要沉积盆地轮廓. 图中主要速度异常：WLVZ：西天山低速区，CLVZ：中天山低速区，THVZ：塔里木高速区，JHVZ：准噶尔高速区. （d, e）体波走时层析成像获得的天山造山带中段 P 波相对速度剖面结果（修改自 Li et al., 2009; Zabelina et al., 2013）. 图案 1 表示向北俯冲的印度板片，图案 2 表示塔里木和哈萨克微陆块

Fig. 7　Seismic velocity structures of Tien Shan and its surroundings. (a-c) Horizontal slices of S-wave velocities at 11, 42, and 60 km depths revealed by full-wave ambient-noise tomography (modified from Lü et al., 2019). Purple solid lines mark locations of Talas-Fergana fault and 80° E. Black dashed lines are outlines of major sedimentary basins. Major velocity anomalies: WLVZ, Western Tien Shan Low-Velocity Zone; CLVZ, Central Tien Shan Low-Velocity Zone; THVZ, Tarim basin High-Velocity Zone; JHVZ, Junggar basin High-Velocity Zone. (d,e) Vertical slices of P-wave velocity perturbations across central Tien Shan constrained by body-wave travel-time tomography (modified from Zabelina et al., 2013; Li et al., 2009). Pattern 1 denotes the subducting Indian slab; pattern 2 shows positions of Tarim and Kazakh lithospheres beneath Tien Shan

al., 2003; 米宁等, 2005; Vinnik et al., 2006; 李昱等, 2007; Omuralieva et al., 2009; Guo et al., 2010; Makarov et al., 2010; Lei, 2011; Zabelina et al., 2013; Gilligan et al., 2014; 刘文学等, 2014; 周铭等, 2014; Li Y et al., 2016; Guo et al., 2017; Khan et al., 2017; Sychev et al., 2018; 蔡妍等, 2019; Li et al., 2019; Lü et al., 2019, 2021; 孔祥艳等, 2021)；相比之下，现有研究对于天山西段深部地壳的波速特征争议较大，高速和低速均有提及，而如果认为天山西段以高速为主，该特征则可能与塔拉斯—费尔干纳断裂两侧不同的构造环境有关（Kosarev et al., 1993; Kufner et al., 2016; Khan et al., 2017; Li et al., 2018; Lü et al., 2019; Liang et al., 2020; Aminov et al., 2020）. 普遍发育的中下地壳低速层表明天山的力学强度相对较低，易于发生强烈变形（蔡妍等，2019；孔祥艳等，2021）. 但另一方面，由于不同研究获得的低速层位置、强度和形态特征具有显著差异，关于该低速层的成因机制仍不十分清楚. 考虑到天山的莫霍面深度较大，低速层可能和中下地壳的增厚直接相关（Zabelina et al., 2013; Aminov et al., 2020）. 另外，上涌到地壳深部的熔体或流体以及地壳矿物在热作用下的脱水熔融也会显著降低地震波速度（Kosarev et al., 1993; Xu et al., 2002; Vinnik et al., 2006; Omuralieva et al., 2009; Guo et al., 2010; Lei, 2011; 刘文学等, 2014; 周铭等, 2014; Guo et al., 2017; Khan et al., 2017; Li Y et al., 2016; Li et al., 2019; Lü et al., 2021）. 也有研究认为山麓地带的低速异常可能反映了南北侧稳定地壳向天山方向的俯冲（Zhao et al., 2003; 李昱等, 2007; Omuralieva et al., 2009; Makarov et al., 2010; Zabelina et al., 2013; Gilligan et al., 2014; Khan et al., 2017; Sychev et al., 2018; 蔡妍等, 2019; 孔祥艳等, 2021)，但现有成像结果所指示的地壳内部速度异常的倾斜形态并不清晰，原因可能和俯冲过程在地壳深度产生的速度异常较小而地壳变形作用又相对复杂有关.

天山上地幔顶部基本延续了其中下地壳的速度结构特征（图 7c）. 整个天山山脉包括其西段表现为大范围的低速异常，反映了大规模的地幔热物质上涌，根据速度异常幅值判断，天山中段尤其是中天山南部是地幔热对流过程最强烈的地区；而位于山体两侧的塔里木、准噶尔和哈萨克岩石圈则相对较厚并以较高的地震波速度为主要特征（Oreshin et al., 2002; Xu et al., 2002; Vinnik et al., 2004; Vinnik et al., 2006; Lei and Zhao, 2007; 李志伟等, 2007; Xu et al., 2007; Koulakov, 2011; Lei, 2011; Bao et al., 2015; Zhou and Lei, 2015; Kufner et al., 2016; Li Y et al., 2016; He and Santosh, 2018; He et al., 2019; Li et al., 2019; Lü et al., 2019; Liang et al., 2020）. 随着深度的增加，天山西段的速度异常逐渐消失，反映该区域构造活动的作用深度较浅（Kufner et al., 2016)；而在天山中东段，仍旧能够观察到显著的速度异常特征，上地幔顶部和地幔转换带之间的多条低速通道表明地幔热对流过程覆盖了整个上地幔，另外也发现有高角度倾斜或近垂直的高速体，可能是拆沉并掉落的天山岩石圈或南北侧的俯冲岩石圈，但关于高速体的形态仍未有统一的认识（Xu et al., 2002; 郭飚等, 2006; 刘洁等, 2007; Lei and Zhao, 2007; Li et al., 2009; Koulakov, 2011; Zabelina et al., 2013; He and Santosh, 2018; Hua et al., 2020）. 例如，Koulakov（2011）及 Lei 和 Zhao（2007）的 P 波走时层析成像研究发现，中天山南北部存在两个形态上差异较大的高速异常体，北部异常与哈萨克岩石圈相连并向南倾斜到 150～200 km 深度，南部异常范围更大、与塔里木岩石圈分离并拆沉到约 500 km 深度（图 7d)；而 Li 等（2009）利用类似方法同样发现中天山两个相向俯冲的高速体，不过其形态特征相近，并且均俯冲到至少 400 km 深度，认为可能是拆沉的天山中部岩石圈（图 7e）.

4　地壳平均波速比与地震波衰减结构特征

地球介质的纵横波速度比（V_P/V_S）与岩石组成关系密切，并且随熔融体熔融程度的提高而增大，但不同的温压条件对该参数的影响较小（Watanabe, 1993; Christensen, 1996）. 大陆地壳的平均波速比一般在 1.75～1.77 上下浮动，并且由于上地壳多由含硅量较大的岩石组成，该深度的波速比相对较低（<1.75），而以铁镁质成分为主的下地壳一般具有较高的波速比（>1.75）（Zandt and Ammon, 1995; Christensen, 1996）. 通过汇总前人利用接收函数 *H-κ* 叠加及其衍生方法得到的天山及其邻区的地壳平均波速比结果（Chen et al., 2010; 刘文学等, 2011; He C et al., 2014; He R et al., 2014; 唐明帅等, 2014; 郑雪刚等, 2016; Wu et al., 2018; Schneider et al., 2019; Cai et al., 2021; Xu et al., 2021; Cheng et al., 2022; Cui et al., 2022）（图 8），我们发现多数台站的地壳波速比位于 1.70～1.80 区间，与全球大陆

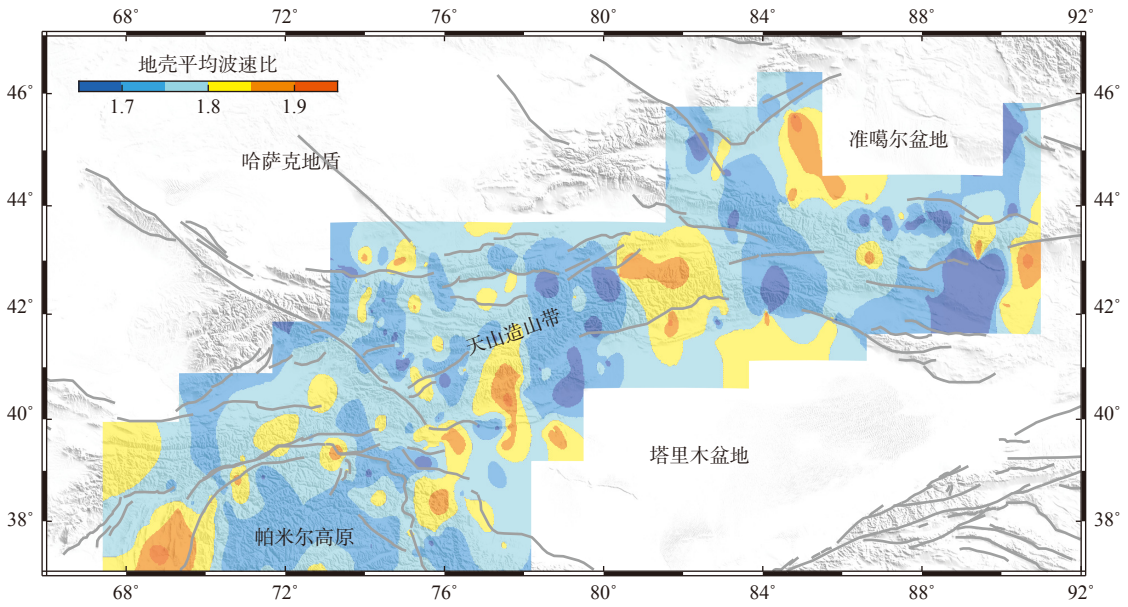

图 8　接收函数方法约束的天山及邻区的地壳平均波速比（整合自 Chen et al., 2010; 刘文学等, 2011; Schneider et al., 2013; He C et al., 2014; He R et al., 2014; 唐明帅等, 2014; 郑雪刚等, 2016; Wu et al., 2018; Schneider et al., 2019; Zhang et al., 2020; Cai et al., 2021; Xu et al., 2021; Cheng et al., 2022; Cui et al., 2022），经克里金插值得到

Fig. 8　Crustal V_P/V_S ratio of Tien Shan and its surroundings from receiver-function studies interpolated using Kriging method (compiled from Chen et al., 2010; Liu et al., 2011; Schneider et al., 2013; He C et al., 2014; He R et al., 2014; Tang et al., 2014; Zheng et al., 2016; Wu et al., 2018; Schneider et al., 2019; Zhang et al., 2020; Cai et al., 2021; Xu et al., 2021; Cheng et al., 2022; Cui et al., 2022)

平均值相近，平均误差 0.06，另有部分台站获得了>1.80 的结果，但分布较为零散. 虽然部分研究认为这些局部的高波速比可以看作天山中下地壳部分熔融或富含流体的证据（Cai et al., 2021; Cui et al., 2022），但其他因素如地壳铁镁质组分增加（刘文学等，2011）或者存在较厚的地表沉积层（Schneider et al., 2019）也可能会导致类似的观测结果，另外考虑到其散落分布的特征，测量误差的影响也不容忽视.

地震波衰减反映了地下介质的非弹性性质，对介质的均匀程度、温度、裂隙分布以及孔隙流体较为敏感（Sato et al., 1989; Dong and Menke, 2017）. 衰减程度一般采用品质因子 Q 表示，Q 值分布与构造活动强度的相关性较好（何静等，2017）. 天山造山带构造变形作用复杂，高热流所指示的地壳生热过程、广泛分布的褶皱系以及可能的部分熔融均会导致入射到该地区的地震波发生强烈的散射衰减，对应低 Q 值；相比之下，塔里木、哈萨克以及部分山间盆地等构造稳定区则主要表现为高 Q 值低衰减（Sarker and Abers, 1999; 徐彦等, 2005; Kopnichev and Sokolova, 2007; Sychev et al., 2018; Ma and Huang, 2020）（图 9）. 但也有部分研究结果显示，塔里木盆地尤其是其北缘盆山过渡带的 Q 值要明显低于天山山脉，认为主要和区域较厚且

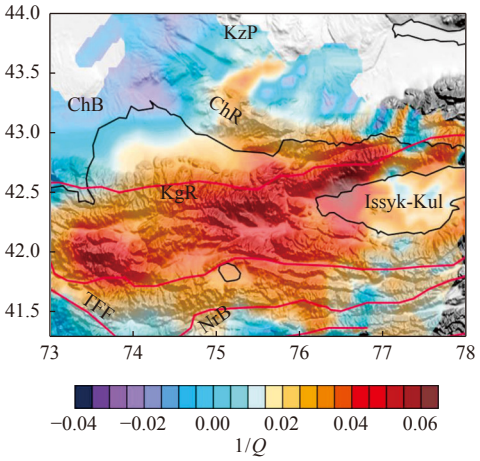

图 9　中天山北部 15-km 深度的 P 波衰减结构（修改自 Sychev et al., 2018）. ChB：邱亚盆地，KzP：哈萨克地盾，ChR：邱亚山脉，KgR：吉尔吉斯山脉，TFF：塔拉斯—费尔干纳断裂，NrB：纳伦盆地，Issyk-Kul：伊塞克湖

Fig. 9　P-wave velocity attenuation at 15 km depth beneath north-central Tien Shan (modified from Sychev et al., 2018). ChB, Chuya basin; KzP, Kazakh shield; ChR, Chuya ridge; KgR, Kyrgyz range; TFF, Talas-Fergana fault; NrB, Naryn basin

松散的沉积层有关，并受到局部的断裂带、破碎带以及频繁地震活动的影响（李金等，2017；赵俊猛等，2003a，2003b）. 此外，现阶段关于天山地区 Q 值结构的深度变化趋势（Sarker and Abers, 1999; 赵俊猛等, 2003a, 2003b; Sychev et al., 2018）以及

频率特性（徐彦等, 2005; 李金等, 2017; Ma and Huang, 2020）仍存有较大争议.

5　天山新生代隆升变形的深部动力学过程

新生代天山的复活再造过程滞后于印度—欧亚板块的初始碰撞（Hendrix et al., 1994; Charreau et al., 2006）. 和其他陆内造山带类似，一般认为天山构造变形的驱动力主要来源于板块边界处的挤压应力（Raimondo et al., 2014），应力经由强硬的塔里木岩石圈向北转移，并最终在流变学性质相对软弱并存有大量薄弱带的天山地区释放（Flesch et al., 2001; Bagdassarov et al., 2011; Huangfu et al., 2021）. 另外，如前所述的大量深部探测结果表明在天山山脉下方可能存在地幔热物质的上涌，该过程导致该处岩石圈力学强度显著降低，为天山的加速隆升创造了有利条件（郭飚等, 2006; 李志伟等, 2007; 刘洁等, 2007; Xu et al., 2007）.

相比于较为明确的构造应力来源，当前科学界对于天山地区的岩石圈变形模式仍未达成统一的认识. 陆内俯冲对于天山新生代造山过程的重要性被众多学者反复强调，一般认为在塔拉斯—费尔干纳断裂西侧沿主帕米尔逆冲断层发生亚洲岩石圈向帕米尔方向的深俯冲（Sippl et al., 2013; Kufner et al., 2016; Schneider et al., 2019），位于俯冲带下盘的西天山以缩短增厚变形作用为主（Kosarev et al., 1993; Khan et al., 2017; Lü et al., 2019）. 而在塔拉斯—费尔干纳断裂东侧，天山的构造环境发生转变，其南部与稳定的塔里木克拉通相接壤，但陆内俯冲仍旧被认为是天山中东段最为重要的深部动力学过程，虽然关于俯冲板片的对称性和精细结构仍存有争议. 一部分学者认为存在南侧塔里木、北侧哈萨克和准噶尔岩石圈向天山方向的双向俯冲（图 10a），并提出“层间插入削减”、“俯冲碰撞拆沉”等模型（Zhao et al., 2003; Lei and Zhao, 2007），但对于块体的俯冲角度（subduction/underthrusting）、俯冲距离以及天山深部地幔高速体的属性也存在不同的观点. 近年来宽频地震剖面的接收函数研究则提出了新的见解，认为天山的变形可能是不对称的（图 10b），陆内俯冲仅发生在天山北部，南天山则在塔里木的北向推挤下发生岩石圈尺度的缩短变形（Li J et al., 2016; Zhang et al., 2020, 2022）. 评估以上模型需要综合考虑研究方法的优缺点、数据集的大小与质量、成像结果的分辨率、地质解释的多解性等多方面因素，但值得一提的是这些动力学模型可能并没有相悖，相当一部分研究就发现天山和南北侧块体的盆山耦合特点存在东西向差异，这可能表明天山不同段落的深部变形过程是不同的. 例如，沿沙雅—布尔津剖面（~85°E），Zhao 等（2003）推测塔里木块体向天山单向俯冲，准噶尔块体与天山以走滑形式相接触；沿库尔勒—

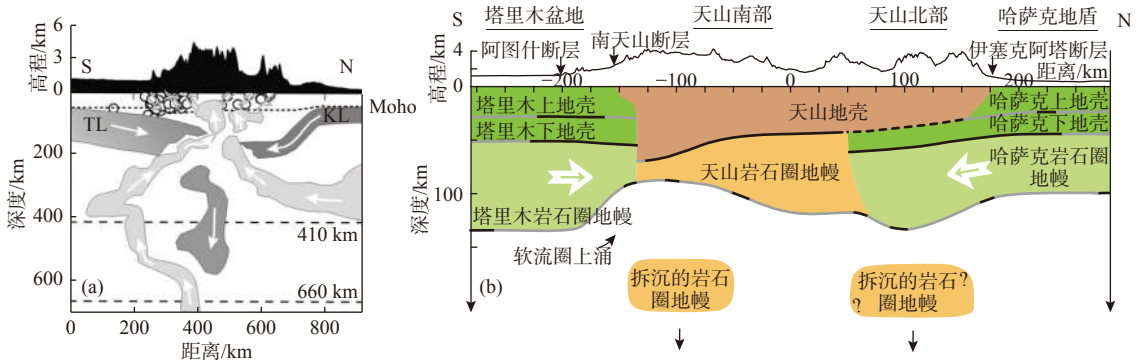

图 10　天山造山带新生代隆升变形的两种模式. （a）双向俯冲模式（修改自 Lei and Zhao, 2007）. 天山两侧的俯冲岩石圈在山脉下方碰撞拆沉，进而引起较大规模地幔上涌. （b）单向俯冲模式（修改自 Zhang et al., 2022）. 由于天山南北侧块体流变学性质的差异性，仅在山脉北部发生哈萨克地盾和准噶尔盆地的单向俯冲，山脉南部以岩石圈缩短增厚变形模式为主并伴随有岩石圈拆沉和地幔上涌

Fig. 10　Schematic illustration of two possible geodynamic scenarios beneath Tien Shan. (a) Two-sided underthrusting (modified from Lei and Zhao, 2007): underthrusted lithospheres collide beneath Tien Shan, which results in breaking-up and dropping-off of the collided lithospheres and, consequently, upwelling of hot deep-mantle materials. (b) One-sided underthrusting (modified from Zhang et al., 2022): Only Kazakh and Junggar lithospheres to the north underthrust beneath Tien Shan. The Tarim lithosphere to the south, conversely, indents rather than subducts under the mountains, resulting in vertically coherent thickening and subsequent foundering of southern Tien Shan lithosphere. Such distinct deformation responses under coherent north-south compression may be controlled by different rheologic properties of bounding terranes

吉木萨尔剖面（~88°E），赵俊猛等（2003a, 2004）提出塔里木与准噶尔向天山方向对冲的接触模式；而沿 MANAS 剖面（~75°E），Zhang 等（2020, 2022）则认为力学性质强硬并受到二叠纪地幔柱活动进一步强化的塔里木克拉通不易发生变形和俯冲，而只有北部的哈萨克岩石圈参与陆内俯冲过程.

6　结语和展望

本文总结了近年来利用地震学探测手段获得的天山造山带及其邻区壳幔间断面形态、各向异性、速度以及衰减结构特征，这些研究结果为揭示天山新生代陆内造山的机理提供了重要约束. 取得的主要共识有：

（1）天山山脉主体和区内沉积盆地的部分结构参数（如地壳厚度、莫霍面形态、地幔转换带厚度、上地壳波速、Q 值结构等）存在明显差异；

（2）天山的地壳上地幔普遍具有各向异性特征，上地幔主偏振方向和造山带走向近似平行，地壳各向异性则呈现出较强的横向变化，研究区可能存在复杂（双层）各向异性结构；

（3）在中下地壳和上地幔顶部，天山大部波速较低，低速异常广泛分布；

（4）陆内俯冲和地幔上涌是天山最重要的深部过程，并且俯冲模式和对流强度可能存在横向变化.

然而，由于我国新疆境内天山的地震数据覆盖相对薄弱，已有研究对于该区壳幔各向异性、LAB 和 MTZ 界面形态的分辨率远远不够. 因此，有必要在我国境内天山布设密集的二维宽频地震台阵、并结合已有数据开展相关研究工作，通过与天山中西段结构特征的对比，我们将有望加深对于天山隆升和陆内造山机理的认识. 另外，目前关于天山地区一些结构参数及其解释的不确定性仍然较大，其原因是多方面的，受到数据集的完备性、反演和解释的多解性、成像结果的分辨率等因素的共同制约. 为解决这一问题，我们既需要对已有结果进行分类评估，也需要在接下来的研究中开展针对多种地球物理资料的联合分析，并结合地质、地球化学等多学科研究成果对动力学演化机制进行探讨.

致谢

感谢三位匿名审稿人建设性的修改建议.

References

Aminov J, Koulakov I, Jakovlev A, et al. 2020. Directions of lithosphere interactions in the Pamir-Hindu Kush junction inferred from anisotropic tomography[J]. Canadian Journal of Earth Sciences, 57(5): 601-616.

Avouac J P, Tapponnier P, Bai M, et al. 1993. Active thrusting and folding along the northern Tien Shan and Late Cenozoic rotation of the Tarim relative to Dzungaria and Kazakhstan[J]. Journal of Geophysical Research, 98(B4): 6755-6804.

Bagdassarov N, Batalev V, Egorova V. 2011. State of lithosphere beneath Tien Shan from petrology and electrical conductivity of xenoliths[J]. Journal of Geophysical Research, 116(B1): B01202.

Balmino G, Vales N, Bonvalot S, et al. 2012. Spherical harmonic modelling to ultra-high degree of Bouguer and isostatic anomalies[J]. Journal of Geodesy, 86: 499-520.

Bao X, Song X, Li J. 2015. High-resolution lithospheric structure beneath Mainland China from ambient noise and earthquake surface-wave tomography[J]. Earth and Planetary Science Letters, 417: 132-141.

Bao X, Eaton D W, Gu Y J. 2016. Rayleigh wave azimuthally anisotropic phase velocity maps beneath western Canada[J]. Journal of Geophysical Research: Solid Earth, 121(3): 1821-1834.

Bao X, Song X, Eaton D W, et al. 2020. Episodic lithospheric deformation in eastern Tibet inferred from seismic anisotropy[J]. Geophysical Research Letters, 47(3): e2019GL085721.

Bao Z W, Gao Y. 2017. Crustal seismic anisotropy in the Tien Shan and adjacent areas[J]. Chinese Journal of Geophysics, 60(4): 1359-1375 (in Chinese).

Bao Z W, Gao Y. 2019. Research progress of seismic anisotropy and dynamic mechanism in the Tienshan region[J]. Earthquake Research in China, 35(4): 589-601 (in Chinese).

Barruol G, Hoffmann R. 1999. Upper mantle anisotropy beneath the Geoscope stations[J]. Journal of Geophysical Research, 104(B5): 10757-10773.

Bump H A, Sheehan A F. 1998. Crustal thickness variations across the northern Tien Shan from teleseismic receiver functions[J]. Geophysical Research Letters, 25(7): 1055-1058.

Burtman V S. 1975. Structural geology of Variscan Tien Shan, USSR[J]. American Journal of Science, 275-A: 157-186.

Cai Y, Wu J P, Ming Y H, et al. 2019. Crust-mantle S wave velocity structures beneath Tianshan area and its deformation analysis[J]. Chinese Journal of Geophysics, 62(11): 4214-4226 (in Chinese).

Cai Y, Wu J, Wang W. 2021. Crustal thickness and Poisson's ratio in Tianshan region from receiver functions[J]. Pure and Applied Geophysics, 178: 3529-3542.

Charreau J, Gilder S, Chen Y, et al. 2006. Magnetostratigraphy of the Yaha section, Tarim Basin (China): 11 Ma acceleration in erosion and uplift of the Tian Shan mountains[J]. Geology, 34(3): 181-184.

Chen Y, Wang L, Mi N, et al. 2005. Shear wave splitting observations in the Chinese Tianshan orogenic belt[J]. Geophysical Research Letters, 32(7): L07306.

Chen Y, Niu F, Liu R, et al. 2010. Crustal structure beneath China from receiver function analysis[J]. Journal of Geophysical Research,

115(B3): B03307.

Chen Y H, Roecker S W, Kosarev G L. 1997. Elevation of the 410 km discontinuity beneath the central Tien Shan: Evidence for a detached lithospheric root[J]. Geophysical Research Letters, 24(12): 1531-1534.

Cheng S, Xiao X, Wu J, et al. 2022. Crustal thickness and V_P / V_S variation beneath continental China revealed by receiver function analysis[J]. Geophysical Journal International, 228(3): 1731-1749.

Cherie S G, Gao S S, Liu K H, et al. 2016. Shear wave splitting analyses in Tian Shan: Geodynamic implications of complex seismic anisotropy[J]. Geochemistry, Geophysics, Geosystems, 17(6): 1975-1989.

Christensen N I. 1996. Poisson's ratio and crustal seismology[J]. Journal of Geophysical Research, 101(B2): 3139-3156.

Crampin S. 1994. The fracture criticality of crustal rocks[J]. Geophysical Journal International, 118(2): 428-438.

Cui Q, Zhou Y, Li J, et al. 2022. Crustal thickness (H) and V_P / V_S ratio (κ) images beneath the central Tien Shan revealed by the H-κ-c method[J]. Tectonophysics, 822: 229157.

Dong M T, Menke W H. 2017. Seismic high attenuation region observed beneath southern New England from teleseismic body wave spectra: Evidence for high asthenospheric temperature without melt[J]. Geophysical Research Letters, 44(21): 10958-10969.

Farra V, Vinnik L P, Romanowicz B, et al. 1991. Inversion of teleseismic S particle motion for azimuthal anisotropy in the upper mantle: A feasibility study[J]. Geophysical Journal International, 106(2): 421-431.

Feng Q Q, Wu Q J, Li Y H, et al. 2012. Shear wave splitting in Xinjiang region[J]. Acta Seismologica Sinica, 34(3): 296-307 (in Chinese).

Flesch L M, Haines A J, Holt W E. 2001. Dynamics of the India-Eurasia collision zone[J]. Journal of Geophysical Research, 106(B8): 16435-16460.

Friederich W. 2003. The S-velocity structure of the east Asian mantle from inversion of shear and surface waveforms[J]. Geophysical Journal International, 153(1): 88-102.

Gan W, Zhang P, Shen Z, et al. 2007. Present-day crustal motion within the Tibetan Plateau inferred from GPS measurements[J]. Journal of Geophysical Research, 112(B8): B08416.

Gao G, Wang H T. 2006. Primary study on S-wave splitting character before and after Wushi earthquake of M_S 6.3[J]. Inland Earthquake, 20(2): 139-142 (in Chinese).

Gao G Y, Nie X H, Long H Y. 2010. Discussion on the characteristics of regional tectonic stress field of Xinjiang from 2003 to 2008[J]. Seismology and Geology, 32(1): 70-79 (in Chinese).

Gao L, Sun D. 2021. Seismic anisotropy beneath the Chinese Mainland: Constraints from shear wave splitting analyses[J]. Earthquake Research Advances, 1(4): 100034.

Gao R, Hou H, Cai X, et al. 2013. Fine crustal structure beneath the junction of the southwest Tian Shan and Tarim Basin, NW China[J]. Lithosphere, 5(4): 382-392.

Gao X, Guo Z, Wang W, et al. 2014. Crustal structure beneath the central Tien Shan from ambient noise tomography[J]. Terra Nova, 26(6): 469-476.

Gao Y J, Cui H H, Zhou Y Z. 2017. Seismic detection of P-wave velocity structure atop MTZ beneath the Central Tian Shan and Tarim Basin[J]. Chinese Journal of Geophysics, 60(1): 98-111 (in Chinese).

Gilligan A, Roecker S W, Priestley K F, et al. 2014. Shear velocity model for the Kyrgyz Tien Shan from joint inversion of receiver function and surface wave data[J]. Geophysical Journal International, 199(1): 480-498.

Guo B, Liu Q Y, Chen J H, et al. 2006. Seismic tomography of the crust and upper mantle structure underneath the Chinese Tianshan[J]. Chinese Journal of Geophysics, 49(6): 1693-1700 (in Chinese).

Guo Z, Gao X, Wang W, et al. 2010. S-wave velocity of the crust around Tianshan Mountains inverted from seismic ambient noise tomography[J]. Chinese Science Bulletin, 55(31): 3590-3598.

Guo Z, Gao X, Yao H, et al. 2017. Depth variations of azimuthal anisotropy beneath the Tian Shan Mt range (NW China) from ambient noise tomography[J]. Journal of Asian Earth Sciences, 138: 161-172.

Guy A, Holzrichter N, Ebbing J. 2017. Moho depth model for the Central Asian Orogenic Belt from satellite gravity gradients[J]. Journal of Geophysical Research: Solid Earth, 122(9): 7388-7407.

He C, Santosh M, Chen X, et al. 2014. Crustal growth and tectonic evolution of the Tianshan orogenic belt, NW China: A receiver function analysis[J]. Journal of Geodynamics, 75: 41-52.

He C, Santosh M. 2018. Role of mantle dynamics in rebuilding the Tianshan Orogenic Belt in NW China: A seismic tomographic investigation[J]. Journal of Geodynamics, 116: 37-46.

He J, Wu Q J, Li Y H, et al. 2017. Developments of earthquake Lg-wave attenuation study and its application in the continental China[J]. Progress in Geophysics, 32(2): 466-475 (in Chinese).

He J, Li Y, Sandvol E, et al. 2019. Tomographic Pn velocity and anisotropy structure in Mongolia and the adjacent regions[J]. Journal of Geophysical Research: Solid Earth, 124(4): 3662-3679.

He R, Shang X, Yu C, et al. 2014. A unified map of Moho depth and V_P/V_S ratio of continental China by receiver function analysis[J]. Geophysical Journal International, 199(3): 1910-1918.

Hearn T M. 1996. Anisotropic Pn tomography in the western United States[J]. Journal of Geophysical Research, 101(B4): 8403-8414.

Heidbach O, Rajabi M, Cui X, et al. 2018. The World Stress Map database release 2016: Crustal stress pattern across scales[J]. Tectonophysics, 744: 484-498.

Helffrich G, Silver P, Given H. 1994. Shear-wave splitting variation over short spatial scales on continents[J]. Geophysical Journal International, 119(2): 561-573.

Helffrich G. 2000. Topography of the transition zone seismic discontinuities[J]. Reviews of Geophysics, 38(1): 141-158.

Hendrix M S, Dumitru T A, Graham S A. 1994. Late Oligocene-early Miocene unroofing in the Chinese Tian Shan: An early effect of the India-Asia collision[J]. Geology, 22(6): 487-490.

Hou H S, Gao R, He R Z, et al. 2012. Shallow-deep tectonic relationship for the junction belt of western part of South Tianshan and Tarim basin—Revealed from preliminary processed deep seismic reflection profile[J]. Chinese Journal of Geophysics, 55(12): 4116-4125 (in Chinese).

Hua Y, Xu Y, Zhao D, et al. 2020. Upper mantle tomography of the Western Junggar: Implications for its geodynamic evolution[J]. Physics of the Earth and Planetary Interiors, 299: 106405.

Huang Z, Wang L, Zhao D, et al. 2011. Seismic anisotropy and mantle dynamics beneath China[J]. Earth and Planetary Science Letters, 306(1-2): 105-117.

Huangfu P, Li Z, Zhang K, et al. 2021. India-Tarim lithospheric mantle collision beneath western Tibet controls the Cenozoic building of Tian Shan[J]. Geophysical Research Letters, 48(14): e2021 GL094561.

Iidaka T, Niu F. 2001. Mantle and crust anisotropy in the eastern China region inferred from waveform splitting of SKS and PpSms[J]. Earth, Planets and Space, 53: 159-168.

Jia C Z, Yang S F, Wei G Q, et al. 2008. Structure characteristics and petroleum bearing prospects of Cenozoic Circum Tibet Plateau Basin and Range System in China[J]. Natural Gas Industry, 28(8): 1-11 (in Chinese).

Jiang L J, Li Y H, Wu Q J. 2010. The shear wave splitting of Central Tien Shan and its implications[J]. Chinese Journal of Geophysics, 53(6): 1399-1408 (in Chinese).

Kaban M K, Yuanda T R. 2014. Density structure, isostatic balance and tectonic models of the Central Tien Shan[J]. Surveys in Geophysics, 35: 1375-1391.

Khan N G, Bai L, Zhao J, et al. 2017. Crustal structure beneath Tien Shan orogenic belt and its adjacent regions from multi-scale seismic data[J]. Science China Earth Sciences, 60(10): 1769-1782.

Ko B, Jung H. 2015. Crystal preferred orientation of an amphibole experimentally deformed by simple shear[J]. Nature Communications, 6: 6586.

Kong X Y, Wu J P, Liu J. 2021. S-wave velocity structure inversed by ambient noise tomography in Xinjiang Tien Shan and its surrounding areas[J]. Earthquake Research in China, 37(1): 43-58 (in Chinese).

Kopnichev Y F, Sokolova I N. 2007. Heterogeneities in the field of short period seismic wave attenuation in the lithosphere of central Tien Shan[J]. Journal of Volcanology and Seismology, 1(5): 333-348.

Kosarev G, Oreshin S, Vinnik L, et al. 2018. Mantle transition zone beneath the central Tien Shan: Lithospheric delamination and mantle plumes[J]. Tectonophysics, 723: 172-177.

Kosarev G L, Petersen N V, Vinnik L P, et al. 1993. Receiver functions for the Tien Shan Analog Broadband Network: Contrasts in the evolution of structures across the Talasso-Fergana Fault[J]. Journal of Geophysical Research, 98(B3): 4437-4448.

Koulakov I. 2011. High-frequency P and S velocity anomalies in the upper mantle beneath Asia from inversion of worldwide traveltime data[J]. Journal of Geophysical Research, 116(B4): B04301.

Kufner S-K, Schurr B, Sippl C, et al. 2016. Deep India meets deep Asia: Lithospheric indentation, delamination and break-off under Pamir and Hindu Kush (Central Asia)[J]. Earth and Planetary Science Letters, 435: 171-184.

Kufner S-K, Eken T, Tilmann F, et al. 2018. Seismic anisotropy beneath the Pamir and the Hindu Kush: Evidence for contributions from crust, mantle lithosphere, and asthenosphere[J]. Journal of Geophysical Research: Solid Earth, 123(12): 10727-10748.

Kumar P, Yuan X, Kind R, et al. 2005. The lithosphere-asthenosphere boundary in the Tien Shan-Karakoram region from S receiver functions: Evidence for continental subduction[J]. Geophysical Research Letters, 32(7): L07305.

Lai Y G, Liu Q Y, Chen J H, et al. 2002. Features of the S-wave splitting and stress field in the Xinjiang Jiashi strong earthquake region[J]. Chinese Journal of Geophysics, 45(1): 83-92 (in Chinese).

Lei J, Zhao D. 2007. Teleseismic P-wave tomography and the upper mantle structure of the central Tien Shan orogenic belt[J]. Physics of the Earth and Planetary Interiors, 162(3-4): 165-185.

Lei J. 2011. Seismic tomographic imaging of the crust and upper mantle under the central and western Tien Shan orogenic belt[J]. Journal of Geophysical Research, 116: B09305.

Lei X Q, Chen Y P, Zhao J M, et al. 2012. Deep probe in the Tianshan orogenic belt and its geodynamics[J]. Progress in Geophysics, 27(2): 417-428 (in Chinese).

Lessing S, Thomas C, Rost S, et al. 2014. Mantle transition zone structure beneath India and western China from migration of PP and SS precursors[J]. Geophysical Journal International, 197(1): 396-413.

Li A, Chen C. 2006. Shear wave splitting beneath the central Tien Shan and tectonic implications[J]. Geophysical Research Letters, 33(22): L22303.

Li J, Zhang J, Zhao X, et al. 2016. Mantle subduction and uplift of intracontinental mountains: A case study from the Chinese Tianshan Mountains within Eurasia[J]. Scientific Reports, 6: 28831.

Li J, Zhou L Q, Wang H L, et al. 2017. Tomography for Q of eastern section of the Tianshan area from high-frequency attenuation of S waves[J]. Earthquake Research in China, 33(2): 229-238 (in Chinese).

Li J, Gao Y, Wang Q. 2021. Anisotropic zoning in the upper crust of the Tianshan Tectonic Belt[J]. Science China Earth Sciences, 64(4): 651-666.

Li M, Lin X, Wu T, et al. 2019. Lithospheric structure of the Tien Shan region constrained by joint inversion of receiver function and Rayleigh wave dispersion[J]. Terra Nova, 31(4): 348-357.

Li S C, Liu Q Y, Chen J H, et al. 2005. Passive broadband seismic array observation across Tianshan[J]. Progress in Geophysics, 20(4): 955-960 (in Chinese).

Li W, Chen Y, Yuan X, et al. 2018. Continental lithospheric subduction and intermediate-depth seismicity: Constraints from S-wave velocity structures in the Pamir and Hindu Kush[J]. Earth and Planetary Science Letters, 482: 478-489.

Li Y, Liu Q Y, Chen J H, et al. 2007. Shear wave velocity structure of the crust and upper mantle underneath the Tianshan orogenic belt[J]. Science in China Series D: Earth Sciences, 37(3): 344-352 (in Chinese).

Li Y, Wu Q, Jiang L, et al. 2010. Complex seismic anisotropic structure beneath the central Tien Shan revealed by shear wave splitting analyses[J]. Geophysical Journal International, 181(3): 1678-1686.

Li Y, Shi L, Gao J. 2016. Lithospheric structure across the central Tien Shan constrained by gravity anomalies and joint inversions of receiver function and Rayleigh wave dispersion[J]. Journal of Asian Earth Sciences, 124: 191-203.

Li Z, Roecker S, Li Z, et al. 2009. Tomographic image of the crust and upper mantle beneath the western Tien Shan from the MANAS broadband deployment: Possible evidence for lithospheric delamination[J]. Tectonophysics, 477(1-2): 49-57.

Li Z W, Xu Y, Roecker S W, et al. 2007. Pn wave velocity structure and anisotropy in the central Tien Shan region[J]. Chinese Journal of Geophysics, 50(4): 1066-1072 (in Chinese).

Liang C, Song X, Huang J. 2004. Tomographic inversion of Pn travel times in China[J]. Journal of Geophysical Research, 109(B11): B11304.

Liang Y, Li L, Liao J, et al. 2020. Interaction of the Indian and Asian plates under the Pamir and Hindu-Kush regions: Insights from 3-D shear wave velocity and anisotropic structures[J]. Geochemistry, Geophysics, Geosystems, 21(8): e2020GC009041.

Liu J, Liu Q Y, Guo B, et al. 2007. Small-scale upper mantle convection and orogeny of Tianshan Mountains in China[J]. Science in China Series D: Earth Sciences, 37(6): 728-735 (in Chinese).

Liu W X, Liu G Z, Zhou G, et al. 2011. Crustal thickness and V_P/V_S ratio variations of Xinjiang and surrounding regions constrained by receiver function stacking[J]. Chinese Journal of Geophysics, 54(8): 2034-2041 (in Chinese).

Liu W X, Liu G Z, Zhou G, et al. 2014. Joint inversion of receiver function and surface wave dispersion for crust and upper mantle S-wave velocity structure beneath Tianshan and its adjacent regions[J]. Acta Seismologica Sinica, 36(1): 20-31 (in Chinese).

Lü Z, Gao H, Lei J, et al. 2019. Crustal and upper mantle structure of the Tien Shan orogenic belt from full-wave ambient noise tomography[J]. Journal of Geophysical Research: Solid Earth, 124(4): 3987-4000.

Lü Z, Gao H, Lei J. 2020. New insight into crustal and lithospheric variability beneath the central Tien Shan (NW China) revealed by P-wave receiver functions[J]. Journal of Asian Earth Sciences, 189: 104187.

Lü Z, Lei J, Zhao L, et al. 2021. Crustal deformation of intermontane basins beneath Central Tien Shan revealed by full-wave ambient noise tomography[J]. Tectonophysics, 821: 229143.

Ma X, Huang Z. 2020. Attenuation of high-frequency P and S waves in the crust of central and western Tien Shan[J]. Pure and Applied Geophysics, 177: 4127-4142.

Makarov V I. 1995. Neotectonics and geodynamics of mountain systems of Central Asia[J]. Quaternary International, 25: 19-23.

Makarov V I, Alekseev D V, Batalev V Y, et al. 2010. Underthrusting of Tarim beneath the Tien Shan and deep structure of their junction zone: Main results of seismic experiment along MANAS Profile Kashgar-Song-Köl[J]. Geotectonics, 44(2): 102-126.

Makeyeva L I, Vinnik L P, Roecker S W. 1992. Shear-wave splitting and small-scale convection in the continental upper mantle[J]. Nature, 358: 144-147.

Malory A O, Bao X, Chen Z. 2022. Crustal shear wave velocity and radial anisotropy beneath Southern Africa from ambient noise tomography[J]. Tectonophysics, 822: 229191.

Mi N, Wang L S, Li H, et al. 2005. Velocity structure of the crust and uppermost mantle in the boundary area of the Tianshan Mountains and the Tarim Basin[J]. Chinese Science Bulletin, 50(4): 363-368 (in Chinese).

Molnar P, Tapponnier P. 1975. Cenozoic tectonics of Asia: Effects of a continental collision: Features of recent continental tectonics in Asia can be interpreted as results of the India-Eurasia collision[J]. Science, 189(4201): 419-426.

Omuralieva A, Nakajima J, Hasegawa A. 2009. Three-dimensional seismic velocity structure of the crust beneath the central Tien Shan, Kyrgyzstan: Implications for large- and small-scale mountain building[J]. Tectonophysics, 465(1-4): 30-44.

Oreshin S, Vinnik L, Peregoudov D, et al. 2002. Lithosphere and asthenosphere of the Tien Shan imaged by S receiver functions[J]. Geophysical Research Letters, 29(8): 1191.

Pasyanos M E, Masters T G, Laske G, et al. 2014. LITHO1.0: An updated crust and lithospheric model of the Earth[J]. Journal of Geophysical Research: Solid Earth, 119(3): 2153-2173.

Raimondo T, Hand M, Collins W J. 2014. Compressional intracontinental orogens: Ancient and modern perspectives[J]. Earth-Science Reviews, 130: 128-153.

Reigber C, Michel G W, Galas R, et al. 2001. New space geodetic constraints on the distribution of deformation in Central Asia[J]. Earth and Planetary Science Letters, 191(1-2): 157-165.

Sarker G, Abers G A. 1999. Lithospheric temperature estimates from seismic attenuation across range fronts in southern and central Eurasia[J]. Geology, 27(5): 427-430.

Sato H, Sacks I S, Murase T, et al. 1989. Qp-melting temperature relation in peridotite at high pressure and temperature: Attenuation mechanism and implications for the mechanical properties of the upper mantle[J]. Journal of Geophysical Research, 94(B8): 10647-10661.

Schneider F M, Yuan X, Schurr B, et al. 2013. Seismic imaging of subducting continental lower crust beneath the Pamir[J]. Earth and Planetary Science Letters, 375: 101-112.

Schneider F M, Yuan X, Schurr B, et al. 2019. The crust in the Pamir: Insights from receiver functions[J]. Journal of Geophysical Research: Solid Earth, 124(8): 9313-9331.

Shin Y H, Xu H, Braitenberg C, et al. 2007. Moho undulations beneath Tibet from GRACE-integrated gravity data[J]. Geophysical Journal International, 170(3): 971-985.

Silver P G, Chan W W. 1991. Shear wave splitting and subcontinental mantle deformation[J]. Journal of Geophysical Research, 96(B10): 16429-16454.

Sippl C, Schurr B, Tympel J, et al. 2013. Deep burial of Asian continental crust beneath the Pamir imaged with local earthquake tomography[J]. Earth and Planetary Science Letters, 384: 165-177.

Sobel E R, Dumitru T A. 1997. Thrusting and exhumation around the margins of the western Tarim basin during the India-Asia collision[J]. Journal of Geophysical Research, 102(B3): 5043-5063.

Steffen R, Steffen H, Jentzsch G. 2011. A three-dimensional Moho depth model for the Tien Shan from EGM2008 gravity data[J]. Tectonics, 30(5): TC5019.

Styron R, Pagani M. 2020. The GEM Global Active Faults Database[J]. Earthquake Spectra, 36(1_suppl): 160-180.

Sun J Z, Xiang Y, Xing X M. 2016. Seismic anisotropy on the upper

mantle in northern Tianshan[J]. Inland Earthquake, 30(3): 243-249 (in Chinese).

Sychev I V, Koulakov I, Sycheva N A, et al. 2018. Collisional processes in the crust of the northern Tien Shan inferred from velocity and attenuation tomography studies[J]. Journal of Geophysical Research: Solid Earth, 123(2): 1752-1769.

Tang M S, Zheng Y, Ge C, et al. 2014. Study on crustal structure in the northeastern Pamir region by P receiver functions[J]. Chinese Journal of Geophysics, 57(10): 3176-3188 (in Chinese).

Tian X, Zhao D, Zhang H, et al. 2010. Mantle transition zone topography and structure beneath the central Tien Shan orogenic belt[J]. Journal of Geophysical Research, 115(B10): B10308.

Vinnik L, Peregoudov D, Makeyeva L, et al. 2002. Towards 3-D fabric in the continental lithosphere and asthenosphere: The Tien Shan[J]. Geophysical Research Letters, 29(16): 1795.

Vinnik L, Deng Y, Kosarev G, et al. 2018. Permian plume beneath Tarim from receiver functions[J]. Solid Earth, 9(5): 1179-1185.

Vinnik L P, Makeyeva L I, Milev A, et al. 1992. Global patterns of azimuthal anisotropy and deformations in the continental mantle[J]. Geophysical Journal International, 111(3): 433-447.

Vinnik L P, Reigber C, Aleshin I M, et al. 2004. Receiver function tomography of the central Tien Shan[J]. Earth and Planetary Science Letters, 225(1-2): 131-146.

Vinnik L P, Aleshin I M, Kaban M K, et al. 2006. Crust and mantle of the Tien Shan from data of the receiver function tomography[J]. Izvestiya, Physics of the Solid Earth, 42(8): 639-651.

Vinnik L P, Aleshin I M, Kiselev S G, et al. 2007. Depth localized azimuthal anisotropy from SKS and P receiver functions: The Tien Shan[J]. Geophysical Journal International, 169(3): 1289-1299.

Wang J, Zhao D. 2008. P-wave anisotropic tomography beneath northeast Japan[J]. Physics of the Earth and Planetary Interiors, 170(1-2): 115-133.

Watanabe T. 1993. Effects of water and melt on seismic velocities and their application to characterization of seismic reflectors[J]. Geophysical Research Letters, 20(24): 2933-2936.

Wolfe C J, Vernon III F L. 1998. Shear-wave splitting at central Tien Shan: Evidence for rapid variation of anisotropic patterns[J]. Geophysical Research Letters, 25(8): 1217-1220.

Wu S, Huang R, Xu Y, et al. 2018. Seismological evidence for a remnant oceanic slab in the western Junggar, Northwest China[J]. Journal of Geophysical Research: Solid Earth, 123(5): 4157-4170.

Wu Y, Bao X, Zhang B, et al. 2022. Seismic evidence for stepwise lithospheric delamination beneath the Tibetan Plateau[J]. Geophysical Research Letters, 49(10): e2022GL098528.

Xiao W, Song D, Windley B F, et al. 2020. Accretionary processes and metallogenesis of the Central Asian Orogenic Belt: Advances and perspectives[J]. Science China Earth Sciences, 63(3): 329-361.

Xiong X S, Gao R, Li Q S, et al. 2011. The deep structure of Tienshan orogenic belt[J]. Progress in Geophysics, 26(6): 1906-1914 (in Chinese).

Xu Q, Zhao J, Yuan X, et al. 2021. Deep crustal contact between the Pamir and Tarim Basin deduced from receiver functions[J]. Geophysical Research Letters, 48(9): e2021GL093271.

Xu Y, Liu F, Liu J, et al. 2002. Crust and upper mantle structure beneath western China from P wave travel time tomography[J]. Journal of Geophysical Research: Solid Earth, 107(B10): 2220.

Xu Y, Mao Y, Hu J F, et al. 2005. Distribution of Lg coda *Q* value in Xinjiang and its adjacent regions[J]. Acta Seismologica Sinica, 27(2): 155-162 (in Chinese).

Xu Y, Li Z, Roecker S W. 2007. Uppermost mantle structure and its relation with seismic activity in the central Tien Shan[J]. Geophysical Research Letters, 34(10): L10304.

Yang Y, Chen J Y, Yang X S, et al. 2010. Does alignment of melt enhance seismic anisotropy beneath Tibet?[J]. Seismology and Geology, 32(1): 59-69 (in Chinese).

Yin A, Nie S, Craig P, et al. 1998. Late Cenozoic tectonic evolution of the southern Chinese Tian Shan[J]. Tectonics, 17(1): 1-27.

Yu Y, Zhao D, Lei J. 2017. Mantle transition zone discontinuities beneath the Tien Shan[J]. Geophysical Journal International, 211(1): 80-92.

Zabelina I V, Koulakov I Y, Buslov M M. 2013. Deep mechanisms in the Kyrgyz Tien Shan orogen (from results of seismic tomography)[J]. Russian Geology and Geophysics, 54(7): 695-706.

Zandt G, Ammon C J. 1995. Continental crust composition constrained by measurements of crustal Poisson's ratio[J]. Nature, 374: 152-154.

Zhang B, Bao X, Xu Y. 2020. Distinct orogenic processes in the south- and north-central Tien Shan from receiver functions[J]. Geophysical Research Letters, 47(6): e2019GL086941.

Zhang B, Bao X, Xu Y. 2022. Seismic anisotropy in central Tien Shan unveils rheology-controlled deformation during intracontinental orogenesis[J]. Geology, 50(7): 812-816.

Zhang P, Shen Z, Wang M, et al. 2004. Continuous deformation of the Tibetan Plateau from global positioning system data[J]. Geology, 32(9): 809-812.

Zhang S, Karato S-I. 1995. Lattice preferred orientation of olivine aggregates deformed in simple shear[J]. Nature, 375: 774-777.

Zhang X, Chen C, Du J S, et al. 2020. Characteristics of Vening Meinesz isostatic gravity anomalies in Tien Shan and surroundings and its dynamic significances[J]. Chinese Journal of Geophysics, 63(10): 3791-3803 (in Chinese).

Zhao J, Liu G, Lu Z, et al. 2003. Lithospheric structure and dynamic processes of the Tianshan orogenic belt and the Junggar basin[J]. Tectonophysics, 376(3-4): 199-239.

Zhao J M, Fan J C, Li Z C. 2003a. *Q*-value structure and geodynamic implication of Korla-Jimsar profile[J]. Science in China Series D: Earth Sciences, 33(3): 202-209 (in Chinese).

Zhao J M, Zhang X K, Deng H Z, et al. 2003b. *Q* value structure of the upper crust along the profile from Baicheng to Da Qaidam[J]. Chinese Journal of Geophysics, 46(4): 503-509 (in Chinese).

Zhao J M, Li Z C, Cheng H G, et al. 2004. Structure of lithospheric density and geomagnetism beneath the Tianshan orogenic belt and their geodynamic implications[J]. Chinese Journal of Geophysics, 47(6): 1061-1067 (in Chinese).

Zhao J Y, Du K F, Yang G H. 2019. Vertical motion characteristics of Tianshan and its adjacent areas measured by continuous GPS[J]. Progress in Geophysics, 34(5): 1835-1841 (in Chinese).

Zheng X, Jiao W, Zhang C, et al. 2010. Short-period Rayleigh-wave

group velocity tomography through ambient noise cross-correlation in Xinjiang, Northwest China[J]. Bulletin of the Seismological Society of America, 100(3): 1350-1355.

Zheng X G, Ma X J, Sun J Z, et al. 2016. Research on crustal structure of seismic stations in Xinjiang different blocks by P receiver functions[J]. Inland Earthquake, 30(4): 314-322 (in Chinese).

Zhou M, Li H Y, Li X F, et al. 2014. Crustal S-wave velocity structure and radial anisotropy in Xinjiang region[J]. China Earthquake Engineering Journal, 36(4): 1047-1058 (in Chinese).

Zhou Z, Lei J. 2015. Pn anisotropic tomography under the entire Tienshan orogenic belt[J]. Journal of Asian Earth Sciences, 111: 568-579.

Zubovich A V, Wang X, Scherba Y G, et al. 2010. GPS velocity field for the Tien Shan and surrounding regions[J]. Tectonics, 29(6): TC6014.

附中文参考文献

鲍子文，高原. 2017. 天山构造带及邻区地壳各向异性[J]. 地球物理学报，60(4)：1359-1375.

鲍子文，高原. 2019. 天山构造带地震各向异性及动力学机制研究进展[J]. 中国地震，35(4)：589-601.

蔡妍，吴建平，明跃红，等. 2019. 新疆天山地区壳幔 S 波速度结构特征及变形分析[J]. 地球物理学报，62(11)：4214-4226.

冯强强，吴庆举，李永华，等. 2012. 新疆地区 S 波分裂研究[J]. 地震学报，34(3)：296-307.

高歌，王海涛. 2006. 乌什 6.3 级地震前、后 S 波分裂特征初步研究[J]. 内陆地震，20(2)：139-142.

高国英，聂晓红，龙海英. 2010. 2003—2008 年新疆区域构造应力场特征探讨[J]. 地震地质，32(1)：70-79.

高雅健，崔辉辉，周元泽. 2017. 中天山和塔里木盆地下方地幔转换带顶部 P 波速度结构探测[J]. 地球物理学报，60(1)：98-111.

郭飚，刘启元，陈九辉，等. 2006. 中国境内天山地壳上地幔结构的地震层析成像[J]. 地球物理学报，49(6)：1693-1700.

何静，吴庆举，李永华，等. 2017. 天然地震 Lg 波衰减研究进展及其在中国大陆地区的应用[J]. 地球物理学进展，32(2)：466-475.

侯贺晟，高锐，贺日政，等. 2012. 西南天山—塔里木盆地结合带浅深构造关系——深地震反射剖面的初步揭露[J]. 地球物理学报，55(12)：4116-4125.

贾承造，杨树锋，魏国齐，等. 2008. 中国环青藏高原新生代巨型盆山体系构造特征与含油气前景[J]. 天然气工业，28(8)：1-11.

江丽君，李永华，吴庆举. 2010. 中天山及邻区 S 波分裂研究及其动力学意义[J]. 地球物理学报，53(6)：1399-1408.

孔祥艳，吴建平，刘靖. 2021. 利用背景噪声层析成像方法反演新疆天山及邻区 S 波速度结构[J]. 中国地震，37(1)：43-58.

赖院根，刘启元，陈九辉，等. 2002. 新疆伽师强震群区的横波分裂与应力场特征[J]. 地球物理学报，45(1)：83-92.

雷显权，陈运平，赵俊猛，等. 2012. 天山造山带深部探测及地球动力学研究进展[J]. 地球物理学进展，27(2)：417-428.

李金，周龙泉，王慧琳，等. 2017. 利用 S 波高频衰减对天山中东段地区地壳 Q 值成像[J]. 中国地震，33(2)：229-238.

李顺成，刘启元，陈九辉，等. 2005. 横跨天山的宽频带流动地震台阵观测[J]. 地球物理学进展，20(4)：955-960.

李昱，刘启元，陈九辉，等. 2007. 天山地壳上地幔的 S 波速度结构[J]. 中国科学 D 辑：地球科学，37(3)：344-352.

李志伟，胥颐，ROECKER S W，等. 2007. 中天山地区的 Pn 波速度结构与各向异性[J]. 地球物理学报，50(4)：1066-1072.

刘洁，刘启元，郭飚，等. 2007. 中国境内天山上地幔小尺度对流与造山作用[J]. 中国科学 D 辑：地球科学，37(6)：728-735.

刘文学，刘贵忠，周刚，等. 2011. 新疆和周边地区地壳厚度和 V_P/V_S 比值变化的接收函数约束[J]. 地球物理学报，54(8)：2034-2041.

刘文学，刘贵忠，周刚，等. 2014. 天山及其邻区地壳上地幔 S 波速度结构的接收函数与面波频散联合反演[J]. 地震学报，36(1)：20-31.

米宁，王良书，李华，等. 2005. 天山和塔里木盆山接合部地壳上地幔速度结构研究[J]. 科学通报，50(4)：363-368.

孙吉泽，向阳，邢喜民. 2016. 北天山上地幔各向异性研究[J]. 内陆地震，30(3)：243-249.

唐明帅，郑勇，葛粲，等. 2014. 帕米尔东北缘地壳结构的 P 波接收函数研究[J]. 地球物理学报，57(10)：3176-3188.

熊小松，高锐，李秋生，等. 2011. 天山造山带的深部结构[J]. 地球物理学进展，26(6)：1906-1914.

徐彦，毛燕，胡家富，等. 2005. 新疆及周边地区 Lg 尾波的 Q 值分布[J]. 地震学报，27(2)：155-162.

杨彧，陈建业，杨晓松，等. 2010. 部分熔融强化了青藏高原地壳的各向异性?[J]. 地震地质，32(1)：59-69.

张星宇，陈超，杜劲松，等. 2020. 天山及邻区 Vening Meinesz 均衡重力异常特征及其动力学意义[J]. 地球物理学报，63(10)：3791-3803.

赵俊猛，樊吉昌，李植纯. 2003a. 库尔勒—吉木萨尔剖面 Q 值结构及其动力学意义[J]. 中国科学 D 辑：地球科学，33(3)：202-209.

赵俊猛，张先康，邓宏钊，等. 2003b. 拜城—大柴旦剖面的上地壳 Q 值结构[J]. 地球物理学报，46(4)：503-509.

赵俊猛，李植纯，程宏岗，等. 2004. 天山造山带岩石圈密度与磁性结构研究及其动力学分析[J]. 地球物理学报，47(6)：1061-1067.

赵静旸，杜凯夫，杨国华. 2019. 连续 GPS 测定的天山及其邻近地区垂向运动特征[J]. 地球物理学进展，34(5)：1835-1841.

郑雪刚，马学军，孙吉泽，等. 2016. 利用 P 波接收函数研究新疆不同地块台站下方地壳结构[J]. 内陆地震，30(4)：314-322.

周铭，李红谊，李信富，等. 2014. 新疆地区地壳 S 波速度结构及径向各向异性研究[J]. 地震工程学报，36(4)：1047-1058.